Unveiling the complex vibronic structure of the canonical adenine cation

Hong Yan Zhao, Kai-Chung Lau, Gustavo Garcia, Laurent Nahon, Stéphane Carniato, Lionel Poisson, Martin Schwell, Muneerah Mogren Al-Mogren, Majdi Hochlaf

PAPER

View Article Online
View Journal | View Issue

Cite this: *Phys. Chem. Chem. Phys.*, 2018, 20, 20756

Unveiling the complex vibronic structure of the canonical adenine cation†

Hong Yan Zhao,[a] Kai-Chung Lau,[a] Gustavo A. Garcia,[b] Laurent Nahon,[b] Stéphane Carniato,[c] Lionel Poisson,[d] Martin Schwell,[e] Muneerah Mogren Al-Mogren[f] and Majdi Hochlaf *[g]

Received 8th May 2018,
Accepted 28th June 2018

DOI: 10.1039/c8cp02930j

rsc.li/pccp

Adenine, a DNA base, exists as several tautomers and isomers that are closely lying in energy and that may form a mixture upon vaporization of solid adenine. Indeed, it is challenging to bring adenine into the gas phase, especially as a unique tautomer. The experimental conditions were tuned to prepare a jet-cooled canonical adenine (9*H*-adenine). This isolated DNA base was ionized by single VUV photons from a synchrotron beamline and the corresponding slow photoelectron spectrum was compared to *ab initio* computations of the neutral and ionic species. We report the vibronic structure of the $X^+\ ^2A''$ (D_0), $A^+\ ^2A'$ (D_1) and $B^+\ ^2A''$ (D_2) electronic states of the 9*H* adenine cation, from the adiabatic ionization energy (AIE) up to AIE + 1.8 eV. Accurate AIEs are derived for the 9*H*-adenine ($\tilde{X}\ ^1A'$) + $h\nu$ — 9*H*-adenine$^+$ ($X^+\ ^2A''$, $A^+\ ^2A'$, $B^+\ ^2A''$) + e^- transitions. Close to the AIE, we fully assign the rich vibronic structure solely to the 9*H*-adenine ($X\ ^1A'$) + $h\nu$ — 9*H*-adenine$^+$ ($X^+\ ^2A''$) transition. Importantly, we show that the lowest cationic electronic states of canonical adenine are coupled vibronically. The present findings are important for understanding the effects of ionizing radiation and the charge distribution on this elementary building block of life, at ultrafast, short, and long timescales.

I. Introduction

Adenine (A) is a DNA base of primary biological importance. The study of the mechanisms underlying the interaction of such compounds with ionizing radiation is crucial in understanding the damage produced by ionizing radiation on larger biomolecules, such as DNA and RNA, and therefore the hazardous genetic mutations potentially mediated by ions, leading, for instance, to an enhanced risk of cancer.[1–4] In addition, the interaction between VUV radiation and nucleobases has also been studied in an astrochemical context,[5–7] because their higher survival rates compared to other small biological molecules, such as amino-acids, means they should be present in interplanetary and interstellar media.

All of the above requires a comprehensive understanding of their electronic structure, their spectroscopy and the accurate determination of their thermochemical data, which explains the large number of studies on their ionization energy (IE) found in the literature since the 1970s (see ref. 8 for a recent review). Briefly, earlier studies consisted of photoelectron spectroscopy,[9–12] photoionization mass spectrometry[13] and electron impact mass spectrometry[14] investigations. The past decade has seen an explosion of physical chemistry literature on this important molecule where modern experimental and theoretical methods have been applied. In the beginning of the 2000s, resonant two-photon ionization laser experiments exploring the mid-UV photochemistry of adenine and other nucleobases were carried out.[15–19] The experimental He I photoelectron spectrum was re-examined in the mid 2000s[20,21] and the first photoionization efficiency spectra using synchrotron radiation as an exciting light source appeared.[6] In the latter work, the mechanisms of the various dissociative ionization reactions in the 6–22 eV range have been described in detail. More recently, single photon ionization of adenine in the gas phase was performed using third generation synchrotron sources.[22,23] These studies confirmed the

[a] *Department of Chemistry, City University of Hong Kong, Kowloon, Hong Kong*
[b] *Synchrotron SOLEIL, L'orme des Merisiers, Saint-Aubin – BP 48 – 91192, Gif-sur-Yvette, Cedex, France*
[c] *Sorbonne Université, CNRS, Laboratoire de Chimie Physique-Matière et Rayonnement, UMR 7614, F-75005 Paris, France*
[d] *LIDYL, CEA, CNRS, Université Paris-Saclay, CEA Saclay 91191, Gif-sur-Yvette, France*
[e] *Laboratoire Interuniversitaire des Systèmes Atmosphériques (LISA), UMR 7583 CNRS, Universités Paris-Est Créteil et Paris Diderot, Institut Pierre et Simon Laplace, 61 Avenue du Général de Gaulle, 94010 Créteil, France*
[f] *Chemistry Department, Faculty of Science, King Saud University, PO Box 2455, Riyadh 11451, Kingdom of Saudi Arabia*
[g] *Université Paris-Est, Laboratoire Modélisation et Simulation Multi Echelle, MSME UMR 8208 CNRS, 5 bd Descartes, 77454 Marne-la-Vallée, France. E-mail: hochlaf@univ-mlv.fr; Fax: +33 160957320; Tel: +33 160957319*

† Electronic supplementary information (ESI) available: The full set of theoretical data, including optimized equilibrium structures of the neutral and ionic adenine species and their energetics. See DOI: 10.1039/c8cp02930j

earlier findings of Trofimov *et al.*[20] and Jochims *et al.*[6] At the same time, theoretical studies using various methods have been performed[22–31] giving insights into the equilibrium geometry and the electronic structure of the adenine cation and its tautomers in their electronic ground and electronically excited states. They allowed an estimation of the vertical and adiabatic ionization energy of these species and helped in assigning the experimental spectra. Nevertheless, some disagreements exist on the nature and the ordering of the cationic excited states.

The most stable tautomer of adenine is 9*H*-adenine (known as canonical adenine), followed by two other tautomers, *i.e.* 3*H*-adenine and 7*H*-adenine, lying at energies of B0.3 eV with respect to 9*H*-adenine according to an earlier DFT study by Fonseca Guerra *et al.*[27] (Scheme 1 and Table 1). Previous experimental studies assumed that gas-phase adenine produced by heating of a solid sample followed by jet-cooling leads efficiently to the predominance of the 9*H*-adenine isomer in the gas phase prior to ionization (see ref. 8 for more details). Nevertheless, this was never established rigorously since, within the experimental conditions of previous studies, contributions to the experimental spectrum (even small) of 3*H* and 7*H*-adenine low lying tautomers could not be fully excluded. For instance, vaporization of 2-hydroxypyridone, a DNA base analogue, leads predominantly to the keto tautomer pyridone in the gas phase, thereby showing that isomerization can happen during vaporization or jet expansion.[32] Also, we showed recently that 5 tautomers are in a mixture upon vaporization of solid cytosine and subsequent jet expansion.[33] This complicates the comprehension of adenine cation spectroscopy, spectral assignments and the determination of adenine thermochemical data (*e.g.* IEs for a specific adenine tautomer). For instance, it is not clear if the observed congestion in the previous photoelectron spectra of adenine is due to complex vibronic structures or the contribution of several tautomers.

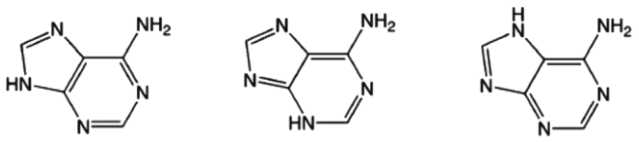

Scheme 1 Structures of 9*H*-adenine, 3*H*-adenine and 7*H*-adenine. Between parentheses, we give the symbols used for their designation in the present study. For common atom numbering, please refer to the ESI.†

Table 1 Relative energies (E_R, eV) and adiabatic ionization energies (AIE, eV) of 9*H*-adenine (9A), of 3*H*-adenine (3A) and of 7*H*-adenine (7A) as computed at the (R)CCSD(T)-F12(b)/cc-pVTZ-F12 (+CV+SR+ZPVE) level. See Table S1 in the ESI for further details

	9A	3A	7A
Relative energies			
E_r[a]	0.000	0.380	0.331
BP86/QZ4P[b]	0.000	0.295	0.325
Adiabatic ionization energies			
Theory			
This work	8.262	8.120	8.462
BP86/QZ4P[b]	8.0274	8.0085	8.2203
MP2/6-31+G(d)[c]	8.18		
B1LYP/6-311+G(d,p)[c]	7.95		
IP-CISD/6-31+G(d)[d]	8.13		
Experiment			
This work	8.264 0.003	—	—
VUV-SPI[e]	8.26		
PIE[f]	8.20 0.05		
PIMS[g]	8.20 0.03		
TPEPICO[h]	8.267 0.005		

[a] Energies are given with respect to 9A. [b] From ref. 27. [c] From ref. 26. [d] EOM-IP-CCSD/cc-pVTZ//IP-CISD/6-31+G(d), ZPE-corrected [oB97X-D/6-31+G(d,p) frequencies]. From ref. 22. [e] From ref. 13. [f] From ref. 22. [g] From ref. 6. [h] From ref. 23.

Here, we present a theoretical investigation of 9*H*-adenine, 3*H*-adenine and 7*H*-adenine using *ab initio* computations to determine the equilibrium structures, the energetics and the frequencies of both the neutral and ionic low lying adenine tautomers (*cf.* ESI†), without any energy scaling. These computations are carried out using density functional theory (DFT) and configuration interaction methods, including explicitly correlated coupled clusters and multi reference configuration interaction techniques. We also recorded the VUV single photon ionization of jet cooled adenine from the adiabatic ionization energy (AIE) up to AIE + 1.8 eV using advanced double imaging electron/ion coincidence (i^{2}PEPICO) techniques in combination with synchrotron radiation. While previous photoelectron experimental spectra consisted of largely unresolved spectra, we measure here, for the first time, a rich vibronic structure in the photoelectron spectrum that is fully and solely assigned to the single tautomer transition 9*H*-adenine + *h*n — 9*H*-adenine$^+$ + e$^-$. The AIEs of the electronic ground state, $X^+\ ^2A''$ (D_0), and those of the two lowest electronic states, $A^+\ ^2A'$ (D_1) and $B^+\ ^2A''$ (D_2), of the 9*H*-adenine$^+$ cation are determined accurately. Also, we show that $A^+\ ^2A'$ and $B^+\ ^2A''$ are coupled vibronically. Implications of these findings for the understanding of the charge redistribution upon VUV light absorption of the canonical adenine DNA base are also discussed.

II. Methods

a. Computations

The present computations have been done using DFT and post Hartree–Fock techniques as implemented in the GAUSSIAN09[34] and MOLPRO (version 2015)[35] packages. They consist of geometry optimizations in the C_1 point group and derivation of the harmonic and anharmonic frequencies of neutral and ionic 9*H*-adenine, 3*H*-adenine and 7*H*-adenine in their electronic ground states. This was done at the PBE0/aug-cc-pVDZ level,[36–38] where all internal coordinates are set free (*i.e.* all relaxed) and where the standard options are used. Then, we carried out single point computations to deduce the accurate energetics. These computations were done at the (R)CCSD(T)-F12(b)/cc-pVTZ-F12 (+CV+SR+ZPVE) level where the neutral and ionic species of adenine tautomers were taken at their optimized PBE0/aug-cc-pVDZ equilibrium geometries. The (R)CCSD(T)-F12(b)/ cc-pVTZ-F12 (+CV+SR+ZPVE) composite scheme corresponds

to (R)CCSD(T)-F12/cc-pVTZ-F12 (approximation b) explicitly correlated computations,[39–41] where we take into account the core-valence (CV, as the difference between CCSD(T)/ cc-pwCVTZ,[42,43] energies with and without considering the core electron correlation), scalar-relativistic (SR, as the difference between CCSD(T)/cc-pVTZ-DK[44–46] and CCSD(T)/cc-pVTZ energies) and zero point vibrational energy (ZPVE as obtained at the PBE0/aug-cc-pVDZ level) corrections. Within the explicitly correlated computations, the cc-pVTZ-F12 explicitly correlated basis sets[47] and the corresponding auxiliary basis sets and density fitting functions[48–51] were used.

For 9*H*-adenine, further computations were carried out for the neutral ground state and for the lowest ionic doublet electronic states using MOLPRO. These computations consisted of geometry optimizations in the C_1 point group, mapping of their potential energy surfaces and harmonic frequency determinations using the state-averaged complete active-space self-consistent field (SA-CASSCF)[52,53] technique and the aug-cc-pVDZ basis set of Dunning and co-workers.[37,54] The active space was constructed using 10 molecular orbitals from HOMO−4 up to LUMO+4 where the core orbitals and the first valence orbitals (up to HOMO−5) were considered as closed orbitals. We performed the explicitly correlated internally contracted Multi Reference Configuration Interaction (MRCI-F12)[55–57] in conjunction with the cc-pVDZ-F12 basis set.[47] The MRCI-F12 space was constructed after considering single and double excitations from all the configurations of the CI expansion of the CASSCF wave functions. Based on these composite schemes, previous comparisons to experimental data[33,58–60] determined the calculated adiabatic ionization energies for the ground state to overestimate the ionization energy by only a few meV (from 2 to 10 meV). For electronically excited states, the accuracy decreases to a few tens of meV, due to the computational limitations of the multireference approach needed to calculate the energy differences to the ground state.

We present in the ESI† the geometrical parameters of neutral and ionic 9A, 3A and 7A species. We also give the full set of their harmonic and anharmonic frequencies and their identification in terms of normal modes. For the thymine DNA basis, Majdi *et al.*[73] showed that the PBE0/aug-cc-pVTZ thymine ground state geometry compares well to those derived using X-ray measurements and using the costly CC/TVZP and CASSCF/aug-cc-pVDZ approaches. For anharmonic frequencies, the PBE0/aug-cc-pVDZ computed values for thymine differ by less than 20–30 cm^{-1} from the most accurate experimental determinations. Thus, the PBE0 achieved accuracy is large enough for the assignment of the vibrationally resolved photoelectron spectra of the DNA bases that we discuss below.

The photoelectron spectrum was simulated as follows. As the process concerns ionization of the neutral closed-shell adenine monomer by removing one electron from the highest doubly occupied molecular orbital to form the $C_5H_5N^+$ cation, the spectrum was simulated considering the change of geometry/normal modes/frequencies between the neutral ground state and the low-energy final (ionized) state. For each normal mode (n), the Huang–Rhys (HR) vibronic coupling parameter, denoted as S_n, which takes into account the difference in equilibrium geometry and evaluates overlaps of the vibrational wave functions of the two shifted harmonic potentials between the initial and final state, was computed. Here, we use the harmonic-oscillator approximation, where each multidimensional vibrational wave function (initial/final) is expressed as a product of $3N - 6$ monodimensional wave functions to calculate the Franck–Condon factors (only the zeroth order term corresponding to a static electronic transition dipole is considered) for excitation from the vibrational ground state of the neutral molecule to the various vibrational states of the ionized molecule. Each $(3N - 6)$ of the normal modes of the final state is projected onto the initial state $(3N - 6)$ normal modes in order to take into account that a mixing of the normal modes occurs during the transition between the initial neutral ground state and the ionized final state within the Franck–Condon (FC) approximation. The transitions between the neutral ground state and the final ionized state were assumed to be vertical and the relative intensities between normal modes of different frequencies were calculated with the Katriel analytic expression.[61] For each kth vibrational mode in the final state, the allowed vibrational level n_k is between 0 and 4. The combination of different $\mathbf{P}_{i¼1}^{3N-6} n_i$ vibrational modes, , was limited to 6. For these computations, the geometries and harmonic frequencies of adenine in its neutral electronic ground state and first (low-lying) cationic state have been calculated with a flexible large cc-pVDZ basis set at a DFT level of theory with the Becke 3-parameter hybrid exchange[62] and the Lee–Yang–Parr[63] gradient-corrected correlation functional (B3LYP). These calculations were executed using the GAMESS(US) package.[64]

b. Experiment

The present experiments were performed at the DESIRS beamline[65] of the French synchrotron SOLEIL. Pure adenine (Z99%) was purchased from Sigma Aldrich and placed inside an in-vacuum temperature-controlled oven heated to 220 1C. This temperature was chosen since it is the minimum value to provide a satisfactory signal-to-noise ratio and at the same time it ensures *a priori* the promotion of a single adenine tautomer (*i.e.* 9*H*-adenine). At this temperature, the 3*H*-adenine/9*H*-adenine and 7*H*-adenine/9*H*-adenine ratios are estimated to be B1 : 8000, according to the calculations shown in Table 1. The adenine vapor was then expanded through a 70 mm nozzle using 1.5 bars of Ar as the carrier gas. The recorded photoion images and derived translational energies for the adenine parent ion did not show any measurable contributions from the dissociative ionization of clusters, with the measured translational temperatures for the adenine around 80 K similar to that of the Ar carrier gas (see Fig. 1). In addition, the lowest energy isomer of the adenine dimer has been shown to be hydrogen-bonded, and one would expect to see a proton transfer prior to dissociation of the parent ion, yielding the fragment $(AH)^+$, and indeed, production of the protonated monomer has been calculated to open at photon

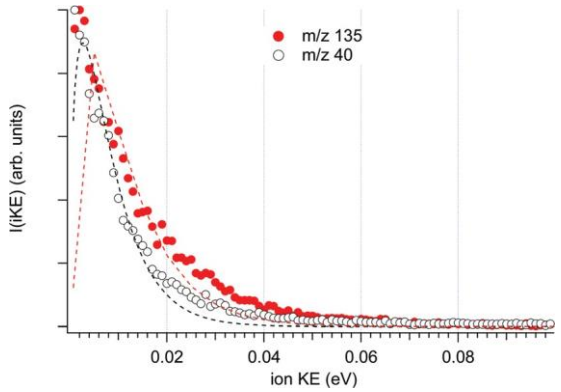

Fig. 1 Ion kinetic energy distributions for the adenine (red filled circles) and argon (black circles) parent ions. The dotted lines represent Boltzmann fits to the data leading to translational temperatures of 85 K for adenine (red dashed line) and 65 K for argon (black dashed line).

energies above 8.97 eV for the most stable isomer.[66] However, in our experiments, although the mass spectrum does show a peak at *m*/*z* 136, its relative abundance corresponds to the 5% expected from the ^{13}C natural abundance in adenine ($C_5H_5N_5$, *m*/*z* 135), which further confirms the lack of dissociative ionization in the parent channel.

After traversing a f = 1 mm skimmer, the molecular beam was crossed at a right angle by the VUV synchrotron radiation. The beamline's monochromator was set to provide a photon bandwidth of 15 meV at 8 eV. A high spectral purity was achieved by filtering out the high harmonics emitted by the undulator with a gas filter[67] located upstream from the monochromator and filled with Ar. The energy scale was autocalibrated to a precision of 3 meV using trace signals from the ionization of Ar, the carrier gas, with second order light. The photon flux was measured using a dedicated photodiode (AXUV, IRD) placed downstream from the photon/sample interaction region and used to correct the data.

The electrons and ions formed at the center of the DELICIOUS3 spectrometer[68] that combines a Velocity Map Imaging (VMI) electron analyzer[69] with a photoion momentum imager were analyzed in coincidence so that the photoelectron images filtered by ion mass and translational energy can be derived in a multiplex manner. The corresponding photoelectron spectra at each photon energy point in the scan were obtained by Abel inversion of these images.[70] In this work, only the photoelectrons from cold adenine (*m*/*z* 135) parent ions having translational energies ⩽50 meV were considered. The 2D photoelectron signal was then obtained as a function of the electron kinetic energy and photon energy (see Fig. 2) from which the ionization threshold can be extracted by choosing the appropriate projection. Then, the slow photoelectron spectrum (SPES) was derived,[32,71] due to its better compromise between the resolution and signal-to-noise ratio with respect to other threshold methods. For instance, here, although photoelectrons between 0 and 50 meV are integrated to build the SPES, the electron resolution is estimated at 10 meV, leading to a total resolution of 18 meV.

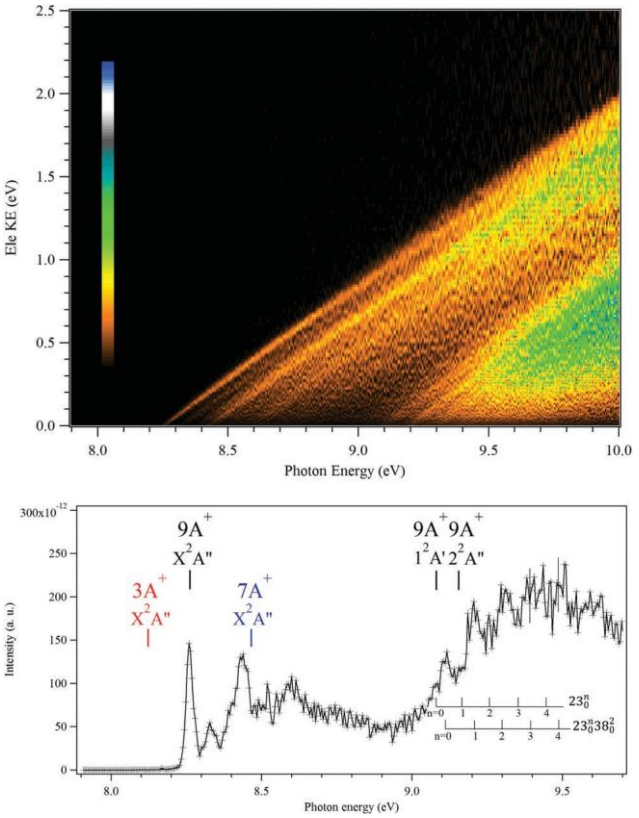

Fig. 2 2D photoionization matrix of adenine providing the electron signal as a function of its kinetic energy and the photon energy. The photon energy step is 5 meV. Lower trace: Slow photoelectron spectrum (SPES) deduced from the 2D spectrum after considering all electrons having kinetic energies between 0 and 50 meV, leading to a total resolution of 18 meV. The vertical combs correspond to the computed adiabatic ionization energies of 9*H*-adenine (9A(X $^1A^{\prime}$) — $9A^+(X^+\ ^2A^{\prime\prime}$, $A^+\ ^2A^{\prime}$, $B^+\ ^2A^{\prime\prime}$)), 3*H*-adenine (3A(X $^1A^{\prime}$) — $3A^+(X^+\ ^2A^{\prime\prime})$) and 7*H*-adenine (7A(X $^1A^{\prime}$) — $7A^+(X^+\ ^2A^{\prime\prime})$) (Tables 1 and 2). We also give the assignment of the bands of the $A^+\ ^2A^{\prime}$ and $B^+\ ^2A^{\prime\prime}$ states. See text.

III. Results and discussion

Fig. 2 (upper panel) displays the 2D photoionization matrix of jet cooled adenine in the 7.9–10.0 eV photon energy region. It shows the number of photoelectron/photoion coincidences *vs.* the photoelectron's kinetic energy and the photon energy. As discussed in ref. 32 and 71 the bright diagonal lines of the slope (hn–IE$_i$)/eKE = 1 correspond to the population of the ith levels of the adenine$^+$ cation by direct ionization. The photoelectron spectrum can be extracted from this matrix in the form of a SPES, which is displayed in Fig. 2 (lower trace). This spectrum starts with an intense peak (at 8.264 0.003 eV) followed by a well resolved rich structure. A second, broader band starting above 9 eV, also shows a few resolved bands superimposed on a mostly structureless background.

The 9A and 3A tautomers of adenine possess a planar electronic ground state, whereas 7A has a C_1 symmetry. Their corresponding ions have a planar structure with a $X^+\ ^2A^{\prime\prime}$ space symmetry due to the ejection of an electron from the outermost ($6a^{\prime\prime}$) molecular orbital (MO) (p type).[27] The AIE of adenine

corresponds to the energy of the adenine ($\tilde{X}\ ^1A^0$) + *h*n — adenine$^+$ ($X^+\ ^2A''$) + e$^-$ photoionization transition, where both the neutral and the ion are in their vibrationless level. At the (R)CCSD(T)-F12(b)/cc-pVTZ-F12 (+CV+SR+ZPVE) level, the AIEs of 9A, 3A and 7A are computed to be 8.262 eV, 8.120 eV and 8.462 eV (Table 1).

The first intense peak in the SPES is measured at 8.264 0.003 eV. This value coincides, within the error bars of the calculations, with our computed AIE of 8.262 eV for 9A, so that we deduce an AIE(9A) = 8.264 0.003 eV. For 3A, the computed AIE is 8.120 eV, and the lack of signal in this region combined with the proven precision of the calculations in the 9A case rules out the contribution of 3A in the present experiment. We also re-calculated the thermodynamic stability of the three tautomers with higher precision than in the earlier work[27] (*cf.* Table 1). In view of these results, we can thus conclude that since 7A is as stable as 3A, it is very unlikely that this tautomer is present in the molecular beam prior to ionization even though definite proof cannot be given here because the calculated AIE, 8.462 eV, falls in a dense region of the SPES. Therefore, we believe that the SPES of Fig. 2 is solely due to 9A photoionization.

Both the newly determined experimental and computed AIE values agree well, while being more precise, with the recent determinations such as that deduced from using the equation-of-motion coupled-cluster (of 8.13 eV),[22] from PIE (of 8.20 0.05 eV),[22] from photoionization mass spectrometry (PIMS) (8.20 0.03 eV)[6] and from Threshold Photoelectron Photoion Coincidence (TPEPICO) (of 8.267 0.005 eV)[23] spectroscopy. Note that the DFT AIE values are off by 0.2 eV compared to ours (Table 1).

Upon ionization of 9A to populate the 9A$^+$ ground state, the main geometrical changes occur for the six and five membered aromatic ring distances. Nevertheless, these changes are relatively small (Fig. 3). Indeed, the bond lengths differ by less than 0.05 Å and the in-plane angles are only slightly affected (by less than 11) (Table S3 of the ESI†). We found also that there is a slight influence of ionization on the out-of-plane angles (*cf.* Table S3, ESI†). Because of the favorable Franck–Condon factors, the photoionization experimental spectrum should therefore consist of relatively short vibrational progressions corresponding to the population of certain vibrational modes of the cation for which the 0–0 origin transition should be the most intense. The measured spectrum is consistent with these findings. Indeed, Fig. 4 displays an expansion of the SPES of 9A in the 7.9–9.0 eV photon energy region. This spectrum presents rich, well resolved structures due to the population of the vibrational levels of 9A$^+$($X^+\ ^2A''$) from the vibrationless ground state of the neutral molecule. Since planar structures are found for the neutral and ionic species (C_s point group), only ionic vibrational states of a^0 symmetry are active upon single photon ionization of 9A. They correspond to the population of the levels of a^0 modes, to even overtones of a$''$ vibrational modes and to their combination modes that are a^0. Fig. 4 also gives a first principles simulation of the SPES. As can be seen in this figure, the SPES close to the AIE $X^+\ ^2A''$ state is relatively well reproduced by considering solely the 9A isomer, confirming

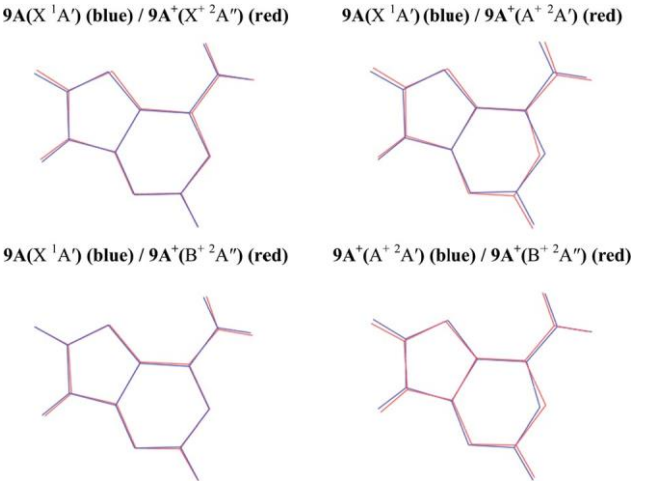

Fig. 3 Superposed structures (optimized at the CASSCF/aug-cc-pVDZ level) of the 9A and 9A$^+$ states under investigation in the present study. 9A($X\ ^1A^0$) is not planar and 9A$^+$($A^+\ ^2A^0$) is in C_s symmetry. For ground states, the matching between the neutral and ionic structures is even better when using PBE0/aug-cc-pVDZ.

once more the predominant population of this form in the jet cooled molecular beam.

Among the 39 vibrational modes of 9A$^+$ (*cf.* Table S6 of the ESI†), the simulation of the SPES leads to a tentative assignment of all the features in the experimental spectrum by considering 6 modes: n^+_9, n^+_{23}, and n^+_{24}, which are of a^0 symmetry and the even quanta of n^+_{32}, n^+_{36}, and n^+_{39}, which are of a$''$ symmetry. The corresponding PBE0/aug-cc-pVDZ anharmonic frequencies are 1489, 729, 600, 644, 428 and 139 (in cm^{-1}), respectively. These modes correspond mostly to the stretching and deformations of the C–NH$_2$ moiety of 9A together with some out-of-plane wagging, twisting and t torsion vibrations of the rings. For some of them, we cannot however fully exclude the contribution of the modes having close energies used for the assignment (Fig. 4). For example, the mode of n^+_{10}, corresponding to the C_4–C_5 stretching is computed at 1446 cm^{-1}, which is close in energy to n^+_9. Since both modes are of a^0 symmetry, they are most likely mixed and form anharmonic resonances (*e.g.* 36^2_0 and 32^2_0 bands). This displaces the energies of the unperturbed levels, as given in Table S6 (ESI†). In our assignment, pure vibrational progressions (*e.g.* 36^n_0, n = 0, 2, 4) or combination modes (*e.g.* $32^2_0 9^1_0$) are found. We are quite confident in the assignments of the fundamentals since they correspond to isolated peaks in the experimental spectra, whereas the deduction may be tentative for the combination and overtone bands because of the congestion of the spectrum at these energies.

It is worth mentioning that there are noticeable intensity deviations between the simulated and experimental curves, particularly above 8.8 eV, where the simulated signal is zero but the measured SPES shows a signal, even in the FC gap region before the first calculated excited state at 9.047 eV (Table 2). These deviations are commonly due to resonant autoionization processes[72] or to vibronic coupling.

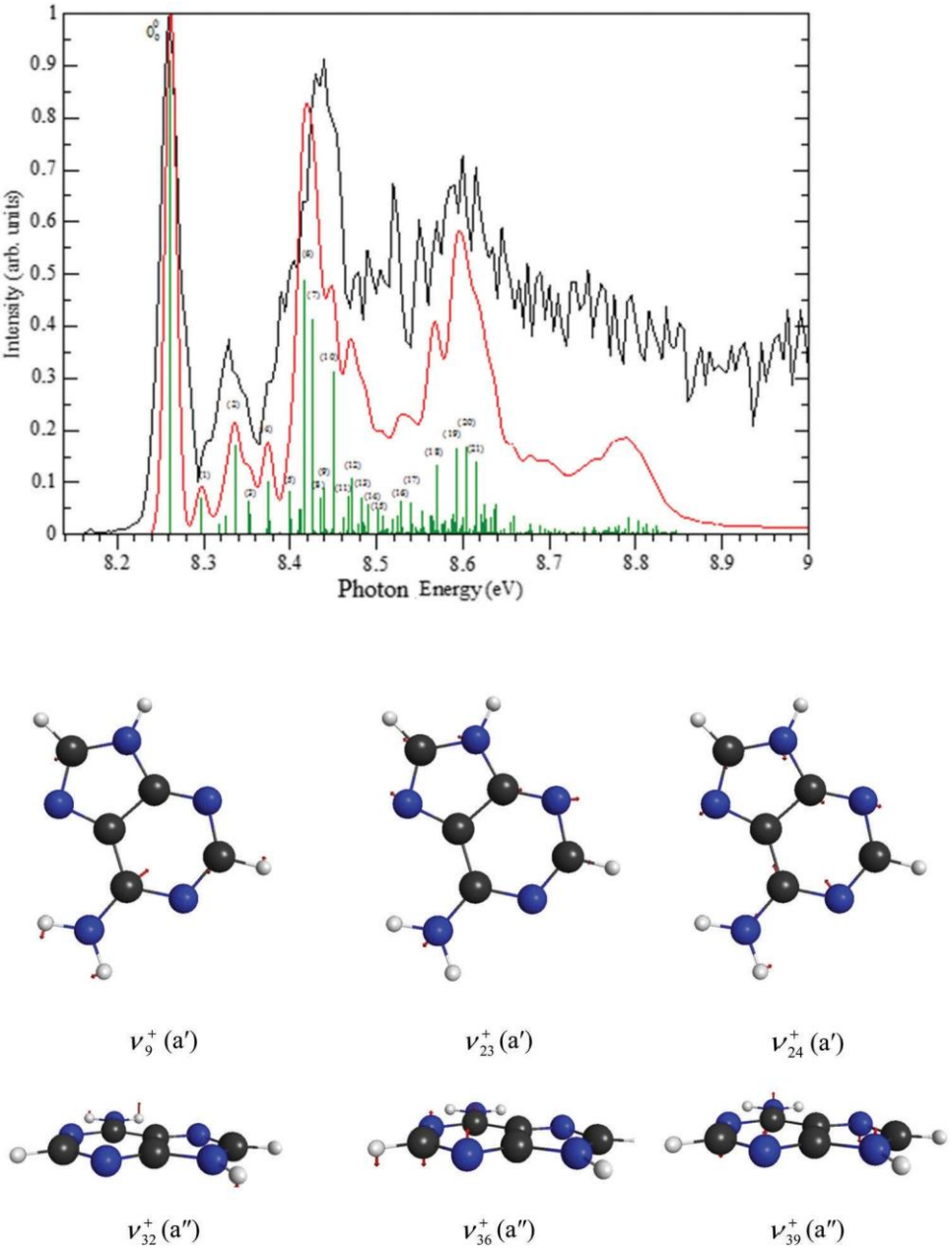

Fig. 4 Upper trace: Simulated (red line) and SPES of 9A (black line) in the 8.1–9 eV range. The tentative assignment of these peaks is given in Table S2 of the ESI.† Lower trace: Normal modes of 9A used for the assignment. The computed intensities are renormalized to that of the 0_0^0 transition.

The assigned peaks in the SPES of Fig. 4 are consistent with the removal of an electron from the outermost p MO of the 9A molecule when forming the ground state of the cation, as stated in ref. 22. For instance, Fig. 5, which displays the bi-dimensional contour plots of the electronic density differ- ences between 9A($X\ ^1A^0$) and $9A^+(X^+\ ^2A^{00})$, shows that there is a lowering of the electron density over the whole molecule and specifically from the C_4–C_5 bond forming the junction between the two rings. Also, we observe a redistribution of the electron density where the CN bonds and H–N_9 are affected.

The AIEs of the $9A^+(A^+\ ^2A^0)$ and $9A^+(B^+\ ^2A^{00})$ excited states were computed at 9.07 and 9.15 eV (Table 2). These states are obtained after ejection of one electron from the ($5a^{00}$) and ($29a^0$) MOs, respectively. Their equilibrium structures are given in Table S4 of the ESI,† and drawn in Fig. 3, where they are superposed onto that of neutral 9A($X\ ^1A^0$). This figure shows that relatively large differences between excited cationic and neutral geometries exist. The planar structure for $A^+\ ^2A^0$ is associated with an imaginary frequency (*i.e.* a transition state), and indeed a slightly lower energy equilibrium structure (all 40 frequencies) with a lower C_1 symmetry is found for this state. Thus, we expect non-favorable Franck–Condon factors for the population of the bands of these states upon ionizing neutral 9A. This may result in long vibrational progressions

Table 2 ... states of 9*H*-adenine$^+$ and their adiabatic ionization energies (AIE, eV), which are compu... neutral species and the electronic excited state of the cation where each species is taken ...

	(R)CCSD(T)-F12/cc-pVTZ-F12 (+CV+SR+ZPVE)[a]	Exp.[d]	
$A^+\ ^2A^{0}$	9.075	9.085	0.005
$A^+\ ^2A^{0}$	—	9.168	0.005
$B^+\ ^2A''$			

[a] Base... 511 (ESI) for more details. [b] SA-CASSCF/aug-cc-pVDZ full optimization (closed 30, occ 40 ... timization (closed 30, occ 40) in the C_1 point group. [d] Position of the first assigned peak ...

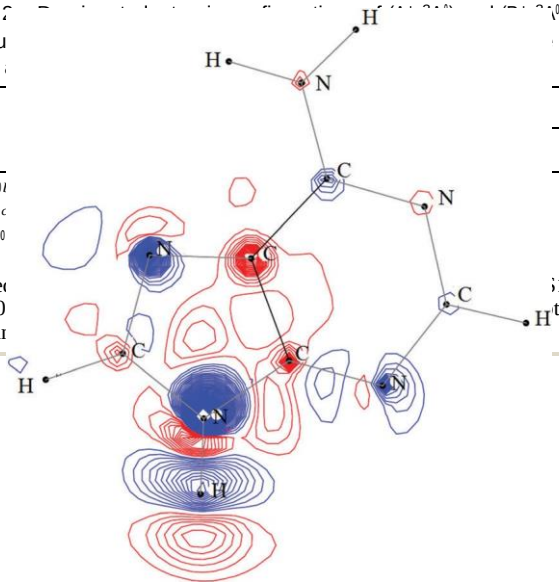

Fig. 5 Difference contour plots of electronic densities between neutral 9A($X\ ^1A^{0}$) and its cation 9A$^+$($X^+\ ^2A''$), where both species are taken at the equilibrium geometry of the neutral. The blue (red) lines correspond to regions where the density in 9A is higher (lower) than in 9A$^+$. We plot the first contour for 0.02 e Bohr^{-3}. The step between the contours is 0.02 e Bohr^{-3}. These computations are done at the CASSCF/aug-cc-pVDZ level and drawn using the MOLDEN package.[75]

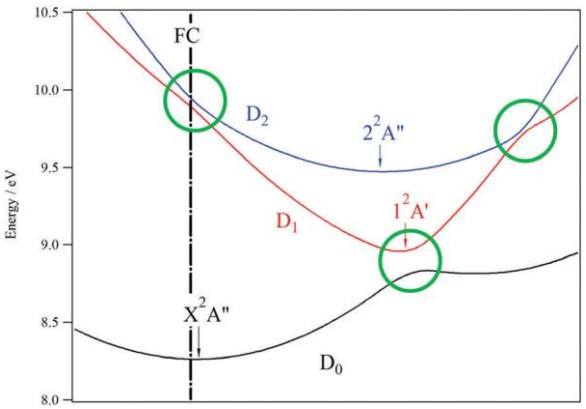

Fig. 6 MRCI-F12/cc-pVDZ-F12 one dimensional cuts of the potentials of the lowest 3 doublet electronic states ($X^+\ ^2A''$, $A^+\ ^2A^{0}$, $B^+\ ^2A''$) of 9-adenine$^+$ for planar configurations along the normal coordinate from $X^+\ ^2A''$ to $A^+\ ^2A^{0}$ equilibrium geometry. These curves are given in energy so that the energy of 9A$^+$($X^+\ ^2A''$) corresponds to the (R)CCSD(T)-F12(b)/cc-pVTZ-F12 (+CV+SR+ZPVE) computed AIE. The vertical arrows indicate the equilibria of 9A$^+$($X^+\ ^2A''$, $A^+\ ^2A^{0}$). The vertical dashed-dotted line corresponds to the middle of the Franck–Condon (FC) region. The green circles indicate the regions of conical intersections.

that may overlap and lead hence to spectral congestion. Moreover, we depict in Fig. 6 the MRCI-F12/cc-pVDZ-F12 one-dimensional cuts of the potentials of the three lowest doublet states of 9A$^+$. This figure points out the existence of conical intersections between 9A$^+$($A^+\ ^2A^{0}$) and 9A$^+$($X^+\ ^2A''$) in the region of the 9A$^+$($A^+\ ^2A^{0}$) minimum. We also found that $B^+\ ^2A''$ is coupled to $A^+\ ^2A^{0}$ vibronically, especially in the Franck–Condon region accessed from the neutral ground state. In the vicinity of these conical intersections, a strong mixing between the wave functions of both states is expected, which again may lead to congestion in the spectra, especially at the threshold. The analysis of the SPES of 9A for photon energies above 9 eV (Fig. 2) – where we expect the population of the upper vibronic levels of the ground cationic state and those of the $A^+\ ^2A^{0}$ and $B^+\ ^2A''$ excited states – confirms these assumptions, showing a broad and a poorly structured band due to congestion.

Based on our calculations, the two peaks observed at 9.085 0.005 and 9.168 0.005 eV in the experimental spectrum are assigned to the AIEs of the $A^+\ ^2A^{0}$ and $B^+\ ^2A''$ excited states in the C_s symmetry, where the curves remain uncoupled. The tail starting around 8.95 eV and the broad structure of the spectrum is attributed to the excitation of modes correlated to the conical intersection, out of C_s symmetry. Close examination of this part of the spectrum shows that there exist two vibronic progressions that could involve mode 23 (a^0) (*i.e.* planar ring breathing) and even the quanta of mode 38, as assigned in Fig. 2. These features are superimposed onto a non-zero real signal, forming a broad profile.

The existence of conical intersections between the doublet states of the adenine cation was suggested by Stolow and co-workers,[21] who performed the time-resolved photoelectron spectroscopy of adenine. Also, these doublet states are coupled. As a consequence, their electron wavefunctions are mixed and exhibit a strong multiconfigurational character. From a theoretical point of view, simple Koopmans' correlations and mono-configurational methodologies are hence not suitable to shed

light on the electronic structure of this DNA base and on the processes occurring upon its interaction with energetic photons. Our findings are of primary importance to understand the fast and ultrafast dynamics of adenine after ejection of an electron from the outermost MOs of this DNA base. Our work suggests that this is accompanied by nuclear and electronic rearrangement phenomena, which are most likely coupled, complicating even more the dynamics upon ionization.

IV. Conclusions

Because of the geometrical changes induced by ionization, the AIEs of the 9A, 3A and 7A tautomers are quite different (by several hundredths of meVs). In this study, we were able to disentangle the vibronic structure of the canonical adenine cation using combined theoretical and experimental SPES techniques. We confirm that the canonical DNA base form is predominantly present in the molecular beam prior to ionization, as expected by the relative energies and experimental conditions. For the ground state of the $9A^+$ cation, the experimental spectrum presents rich vibrational structures that were assigned *via* the good agreement found with a pure first principles simulated spectrum that goes beyond the usual Franck–Condon approximation. We also derived, unambiguously, the AIEs of $X^+\,^2A^{00}$, $A^+\,^2A^0$ and $B^+\,^2A^{00}$ of the $9A^+$ cation with unprecedented precision. Such well-defined AIEs are available only for thymine[73] and some cytosine tautomers.[33] The spectrum for the excited doublet excited states is complex and shows band overlaps and congestion. The origins of such congestions were examined. Specifically, we identified conical intersections between these states. These findings are important to fully understand the effects of ionizing radiation in this DNA base and the corresponding induced dynamics at ultrashort, short, and long timescales,[74] which are of great relevance for the understanding of the multi-timescale cascading events associated with radiation damage.

Conflicts of interest

There are no conflicts to declare.

Acknowledgements

The authors extend their appreciation to the International Scientific Partnership Program (ISPP) at King Saud University for funding this research work through ISPP# 0045. We are indebted to the general technical staff of Synchrotron Soleil for running the facility under proposal #20150956. We would like also to thank Jean-François Gil for his technical help on the SAPHIRS molecular beam chamber. We gratefully acknowledge the support of the COST Action CM1405 entitled MOLIM: Molecules in Motion.

References

1 U. Hagen, Current Aspects on the Radiation Induced Base Damage in DNA, *Radiat. Environ. Biophys.*, 1986, 25, 261–271.
2 A. Kumar and M. D. Sevilla, Proton-Coupled Electron Transfer in DNA on Formation of Radiation-Produced Ion Radicals, *Chem. Rev.*, 2010, 110, 7002–7023.
3 N. Shikazono, M. Noguchi, K. Fujii, A. Urushibara and A. Yokoya, The Yield, Processing, and Biological Consequences of Clustered DNA Damage Induced by Ionizing Radiation, *J. Radiat. Res.*, 2009, 50, 27–36.
4 G. G. Gómez-Tejedor and M. C. Fuss, *Radiation Damage in Biomolecular Systems*, Springer, Dordrecht Heidelberg London New York, 2012.
5 S. Pilling, D. P. P. Andrade, R. B. de Castilho, R. L. Cavasso-Filho, A. F. Lago, L. H. Coutinho, G. B. B. de Souza, H. M. Boechat-Roberty and A. Naves de Brito, Survival of amino acids and nucleobases in space radiations conditions, *Proc. Int. Astron. Union*, 2008, 4, 371–376.
6 H.-W. Jochims, M. Schwell, H. Baumgärtel and S. Leach, Photoion mass spectrometry of adenine, thymine and uracil in the 6–22 eV photon energy range, *Chem. Phys.*, 2005, 314, 263–282.
7 M. Schwell, H.-W. Jochims, H. Baumgärtel, F. Dulieu and S. Leach, VUV photochemistry of small biomolecules, *Planet. Space Sci.*, 2006, 54, 1073–1085.
8 M. Schwell and M. Hochlaf, Photoionization spectroscopy of nucleobases and analogues in the gas phase using synchrotron radiation as excitation light source, *Top. Curr. Chem.*, 2015, 355, 155–208.
9 N. S. Hush and A. S. Cheung, Ionization potentials and donor properties of nucleic acid bases and related compounds, *Chem. Phys. Lett.*, 1975, 34, 11–13.
10 S. Peng, A. Pavda and P. R. LeBreton, Ultraviolet photoelectron studies of biological purines: the valence electronic structure of adenine, *Proc. Natl. Acad. Sci. U. S. A.*, 1976, 73, 2966–2968.
11 J. Lin, C. Yu, S. Peng, I. Akiyama, K. Li, K. L. Li and P. R. LeBreton, Ultraviolet photoelectron studies of the ground-state electronic structure and gas-phase tautomerism of purine and adenine, *J. Am. Chem. Soc.*, 1980, 102, 4627–4631.
12 S. Urano, X. Yang and P. R. LeBreton, UV Photoelectron and Quantum Mechanical Characterization of DNA and RNA Bases: Valence Electronic Structures of Adenine, 1,9-Dimethylguanine, 1-Methylcytosine, Thymine and Uracil, *J. Mol. Struct.*, 1989, 214, 315–328.
13 V. M. Orlov, A. N. Smirnov and Y. M. Varshavsky, Ionization potentials and electron-donor ability of nucleic acid babes and their analogues, *Tetrahedron Lett.*, 1976, 17, 4377–4378.
14 J. M. Rice and G. O. Dudek, Mass spectra of nucleic acid derivatives. II. Guanine, adenine, and related compounds, *J. Am. Chem. Soc.*, 1967, 89, 2719–2725.
15 N. J. Kim, G. Jeong, Y. S. Kim, J. Sung and S. K. Kim, Resonant two-photon ionization and laser induced fluorescence spectroscopy of jet-cooled adenine, *J. Chem. Phys.*, 2000, 113, 10051.

16 C. Plützer, E. Nir, M. S. de Vries and K. Kleinermanns, IR-UV double-resonance spectroscopy of the nucleobase adenine, *Phys. Chem. Chem. Phys.*, 2001, 3, 5466–5469.
17 E. Nir, K. Kleinermanns, L. Grace and M. S. de Vries, On the Photochemistry of Purine Nucleobases, *J. Phys. Chem. A*, 2001, 105, 5106–5110.
18 E. Nir, C. Plützer, K. Kleinermanns and M. S. de Vries, Properties of isolated DNA bases, base pairs and nucleosides examined by laser spectroscopy, *Eur. Phys. J. D*, 2002, 20, 317–329.
19 K. Kleinermanns, D. Nachtigallová and M. S. de Vries, Excited state dynamics of DNA bases, *Int. Rev. Phys. Chem.*, 2013, 32, 308–342.
20 A. B. Trofimov, J. Schirmer, V. B. Kobychev, A. W. Potts, D. M. P. Holland and L. Karlsson, Photoelectron Spectra of the Nucleobases Cytosine, Thymine and Adenine, *J. Phys. B: At., Mol. Opt. Phys.*, 2006, 39, 305.
21 H. Satzger, D. Townsend and A. Stolow, Reassignment of the low lying cationic states in gas phase adenine and 9-methyl adenine, *Chem. Phys. Lett.*, 2006, 430, 144–148.
22 K. B. Bravaya, O. Kostko, S. Dolgikh, A. Landau, M. Ahmed and A. I. Krylov, Electronic Structure and Spectroscopy of Nucleic Acid Bases: Ionization Energies, Ionization-Induced Structural Changes, and Photoelectron Spectra, *J. Phys. Chem. A*, 2010, 114, 12305–12317.
23 D. Touboul, F. Gaie-Levrel, G. Garcia-Macias, L. Nahon, L. Poisson, M. Schwell and M. Hochlaf, VUV photoionization of gas phase adenine and cytosine: a comparison between oven and aerosol vaporization, *J. Chem. Phys.*, 2013, 138, 094203.
24 M. Hanus, M. Kabeláč, J. Rejnek, F. Ryjacek and P. Hobza, Correlated ab Initio Study of Nucleic Acid Bases and Their Tautomers in the Gas Phase, in a Microhydrated Environment, and in Aqueous Solution. Part 3. Adenine, *J. Phys. Chem. B*, 2004, 108, 2087–2097.
25 M. Piacenza and S. Grimme, Systematic Quantum Chemical Study of DNA-Base Tautomers, *J. Comput. Chem.*, 2004, 25, 83–99.
26 R. Improta, G. Scalmani and V. Barone, Radical cations of DNA bases: some insights on structure and fragmentation patterns by density functional methods, *Int. J. Mass Spectrom.*, 2000, 201, 321–336.
27 C. Fonseca Guerra, F. M. Bickelhaupt, S. Saha and F. Wang, Adenine Tautomers: Relative Stabilities, Ionization Energies, and Mismatch with Cytosine, *J. Phys. Chem. A*, 2006, 110, 4012–4020.
28 S. Wang and H. F. Schaefer III, The small planarization barriers for the amino group in the nucleic acid bases, *J. Chem. Phys.*, 2006, 124, 044303.
29 D. Roca-Sanjuan, M. Rubio, M. Merchan and L. J. Serrano-Andrés, Ab initio determination of the ionization potentials of DNA and RNA nucleobases, *J. Chem. Phys.*, 2006, 125, 084302.
30 E. Cauët, D. Dehareng and J. Liévin, Ab Initio Study of the Ionization of the DNA Bases: Ionization Potentials and Excited States of the Cations, *J. Phys. Chem. A*, 2006, 110, 9200–9211.
31 O. Dolgounitcheva, V. G. Zakrzewski and J. V. Ortiz, Vertical Ionization Energies of Adenine and 9-Methyl Adenine, *J. Phys. Chem. A*, 2009, 113, 14630–14635.
32 J. C. Poully, J. P. Schermann, N. Nieuwjaer, F. Lecomte, G. Grégoire, C. Desfrançois, G. A. Garcia, L. Nahon, D. Nandi, L. Poisson and M. Hochlaf, Photoionization of 2-pyridone and 2-hydroxypyridine, *Phys. Chem. Chem. Phys.*, 2010, 12, 3566–3572.
33 Z. Chen, K.-C. Lau, G. A. Garcia, L. Nahon, D. K. Božanić, L. Poisson, M. Mogren Al-Mogren, M. Schwell, J. S. Francisco, A. Bellili and M. Hochlaf, Identifying cytosine-specific isomers *via* high-accuracy single photon ionization, *J. Am. Chem. Soc.*, 2016, 138, 16596–16599.
34 M. J. Frisch, G. W. Trucks, H. B. Schlegel, G. E. Scuseria, M. A. Robb, J. R. Cheeseman, G. Scalmani, V. Barone, B. Mennucci and G. A. Petersson, *et al.*, *Gaussian 09, revision A.02*, Gaussian, Inc., Wallingford, CT, 2009.
35 H.-J. Werner, P. J. Knowles, G. Knizia, F. R. Manby, M. Schütz, P. Celani, T. Korona, R. Lindh, A. Mitrushenkov and G. Rauhut, *et al.*, *MOLPRO, ab initio programs package*, 2015, http://www.molpro.net.
36 C. Adamo and V. Barone, Toward Reliable Density Functional Methods Without Adjustable Parameters: The PBE0 Model, *J. Chem. Phys.*, 1999, 110, 6158–6170.
37 T. H. Dunning, Gaussian Basis Sets for Use in Correlated Molecular Calculations. I. The Atoms Boron through Neon and Hydrogen, *J. Chem. Phys.*, 1989, 90, 1007–1023.
38 R. A. Kendall, T. H. Dunning and R. J. Harrison, Electron Affinities of the First-Row Atoms Revisited. Systematic Basis Sets and Wave Functions, *J. Chem. Phys.*, 1992, 96, 6796–6806.
39 T. B. Adler, G. Knizia and H.-J. Werner, A simple and efficient CCSD(T)-F12 approximation, *J. Chem. Phys.*, 2007, 127, 221106.
40 H.-J. Werner, G. Knizia and F. R. Manby, Explicitly correlated coupled cluster methods with pair-specific geminals, *Mol. Phys.*, 2011, 109, 407–417.
41 G. Knizia, T. B. Adler and H.-J. Werner, Simplified CCSD(T)-F12 methods: theory and benchmarks, *J. Chem. Phys.*, 2009, 130, 054104.
42 G. Rauhut, G. Knizia and H.-J. Werner, Accurate calculation of vibrational frequencies using explicitly correlated coupled-cluster theory, *J. Chem. Phys.*, 2009, 130, 054105.
43 K. A. Peterson and T. H. Dunning, Accurate correlation consistent basis sets for molecular core–valence correlation effects: The second row atoms Al–Ar, and the first row atoms B–Ne revisited, *J. Chem. Phys.*, 2002, 117, 10548.
44 M. Douglas and N. M. Kroll, Quantum electrodynamical corrections to the fine structure of helium, *Ann. Phys.*, 1974, 82, 89–155.
45 G. Jansen and B. A. Hess, Revision of the Douglas-Kroll transformation, *Phys. Rev. A: At., Mol., Opt. Phys.*, 1989, 39, 6016–6017.
46 W. A. de Jong, R. J. Harrison and D. A. Dixon, Parallel Douglas–Kroll energy and gradients in NWChem: estimating scalar relativistic effects using Douglas–Kroll contracted basis sets, *J. Chem. Phys.*, 2001, 114, 48.

47 K. A. Peterson, T. B. Adler and H.-J. Werner, Systematically convergent basis sets for explicitly correlated wavefunctions: the atoms H, He, B–Ne, and Al–Ar, *J. Chem. Phys.*, 2008, 128, 084102.
48 F. A. Weigend, A fully direct RI-HF algorithm: implementation, optimised auxiliary basis sets, demonstration of accuracy and efficiency, *Phys. Chem. Chem. Phys.*, 2002, 4, 4285–4291.
49 C. Hättig, Optimization of auxiliary basis sets for RI-MP2 and RI-CC2 calculations: core-valence and quintuple-z basis sets for H to Ar and QZVPP basis sets for Li to Kr, *Phys. Chem. Chem. Phys.*, 2005, 7, 59–66.
50 W. Klopper, Highly accurate coupled-cluster singlet and triplet pair energies from explicitly correlated calculations in comparison with extrapolation techniques, *Mol. Phys.*, 2001, 99, 481–507.
51 K. E. Yousaf and K. A. Peterson, Auxiliary RI Basis Sets (OptRI) matched to cc-pVnZ-F12:H, B–Ne, Al–Ar, *J. Chem. Phys.*, 2008, 129, 184108.
52 P. J. Knowles and H.-J. Werner, An Efficient Second-order MC SCF Method for Long Configuration Expansions, *Chem. Phys. Lett.*, 1985, 115, 259–267.
53 H.-J. Werner and P. J. Knowles, A Second Order Multiconfiguration SCF Procedure with Optimum Convergence, *J. Chem. Phys.*, 1985, 82, 5053–5063.
54 T. H. Dunning and R. J. Harrison, Electron Affinities of the First-Row Atoms Revisited. Systematic Basis Sets and Wave Functions, *J. Chem. Phys.*, 1992, 96, 6796–6806.
55 T. Shiozaki, G. Knizia and H.-J. Werner, Explicitly correlated multireference configuration interaction: MRCI-F12, *J. Chem. Phys.*, 2011, 134, 034113.
56 T. Shiozaki and H.-J. Werner, Explicitly correlated multireference configuration interaction with multiple reference functions: Avoided crossings and conical intersections, *J. Chem. Phys.*, 2011, 134, 184104.
57 T. Shiozaki and H.-J. Werner, Multireference explicitly correlated F12 theories, *Mol. Phys.*, 2013, 111, 607–630.
58 Y. Pan, K.-C. Lau, L. Poisson, G. A. Garcia, L. Nahon and M. Hochlaf, Slow Photoelectron Spectroscopy of 3-Hydroxyisoquinoline, *J. Phys. Chem. A*, 2013, 117, 8095–8102.
59 Y. Pan, K.-C. Lau, M. M. Al-Mogren, A. Mahjoub and M. Hochlaf, Theoretical studies of 2-quinolinol: geometries, vibrational frequencies, isomerization, tautomerism, and excited states, *Chem. Phys. Lett.*, 2014, 613, 29–33.
60 M. Hochlaf, Advances in spectroscopy and dynamics of small and medium sized molecules and clusters, *Phys. Chem. Chem. Phys.*, 2017, 19, 21236–21261.
61 J. Katriel, Second quantization and the general two-centre harmonic oscillator integrals, *J. Phys. B: At. Mol. Phys.*, 1970, 3, 1315.
62 A. D. Becke, Density-functional thermochemistry. III. The role of exact exchange, *J. Chem. Phys.*, 1993, 98, 5648.
63 C. Lee, W. Yang and R. G. Parr, Development of the Colle-Salvetti correlation-energy formula into a functional of the electron density, *Phys. Rev. B: Condens. Matter Mater. Phys.*, 1988, 37, 785–789.
64 M. W. Schmidt, K. K. Baldridge, J. A. Boatz, S. T. Elbert, M. S. Gordon, J. J. Jensen, S. Koseki, N. Matsunaga, K. A. Nguyen, S. Suand, T. L. Windus, M. Dupuis and J. A. Montgomery, General atomic and molecular electronic structure system, *J. Comput. Chem.*, 1993, 14, 1347–1363.
65 L. Nahon, N. de Oliveira, G. A. Garcia, J.-F. Gil, B. Pilette, O. Marcouillé, B. Lagarde and F. Polack, DESIRS: a state-of-the-art VUV beamline featuring high resolution and variable polarization for spectroscopy and dichroism at SOLEIL, *J. Synchrotron Radiat.*, 2012, 19, 508–520.
66 K. B. Bravaya, O. Kostko, M. Ahmed and A. I. Krylov, The effect of p-stacking, H-bonding, and electrostatic interactions on the ionization energies of nucleic acid bases: adenine–adenine, thymine–thymine and adenine–thymine dimers, *Phys. Chem. Chem. Phys.*, 2010, 12, 2292.
67 B. Mercier, M. Compin, C. Prevost, G. Bellec, R. Thissen, O. Dutuit and L. Nahon, Experimental and theoretical study of a differentially pumped absorption gas cell used as a low energy-pass filter in the vacuum ultraviolet photon energy range, *J. Vac. Sci. Technol., A*, 2000, 18, 2533.
68 G. A. Garcia, B. K. Cunha de Miranda, M. Tia, S. Daly and L. Nahon, DELICIOUS III: a multipurpose double imaging particle coincidence spectrometer for gas phase vacuum ultraviolet photodynamics studies, *Rev. Sci. Instrum.*, 2013, 84, 053112.
69 A. T. J. B. Eppink and D. H. Parker, Velocity map imaging of ions and electrons using electrostatic lenses: application in photoelectron and photofragment ion imaging of molecular oxygen, *Rev. Sci. Instrum.*, 1997, 68, 3477.
70 G. A. Garcia, L. Nahon and I. Powis, Two-dimensional charged particle image inversion using a polar basis function expansion, *Rev. Sci. Instrum.*, 2004, 75, 4989.
71 M. Briant, L. Poisson, M. Hochlaf, P. de Pujo, M.-A. Gaveau and B. Soep, Ar2 Photoelectron Spectroscopy Mediated by Autoionizing States, *Phys. Rev. Lett.*, 2012, 109, 193401.
72 T. Baer, Vacuum UV Photophysics and Photoionization Spectroscopy, *Annu. Rev. Phys. Chem.*, 1989, 40, 637–669.
73 Y. Majdi, M. Hochlaf, Y. Pan, K.-C. Lau, L. Poisson, G. A. Garcia, L. Nahon, M. Mogren Al-Mogren and M. Schwell, Theoretical and Experimental Photoelectron Spectroscopy Characterization of the Ground State of Thymine Cation, *J. Phys. Chem. A*, 2015, 119, 5951–5958.
74 H. Satzger, D. Townsend, M. Z. Zgierski, S. Patchkovskii, S. Ullrich and A. Stolow, Primary processes underlying the photostability of isolated DNA bases: adenine, *Proc. Natl. Acad. Sci. U. S. A.*, 2006, 103, 10196–10201.
75 G. Schaftenaar and J. H. Noordik, *J. Comput.-Aided Mol. Des.*, 2000, 14, 123–134.